Mobile Energy Storage for Inverter-dominated Isolated Microgrids Resiliency Enhancement Through Maximizing Loadability and Seamless Reconfiguration

Wael El-Sayed, *Member*, *IEEE*, Ahmed Awad, *Senior Member*, *IEEE*, Maher Azzouz, *Senior Member*, *IEEE*, Mostafa Shaaban, *Senior Member*, *IEEE*, and Ehab El-Saadany, *Fellow*, *IEEE*

***Abstract*—Inverter-dominated isolated/islanded microgrids (IDIMGs) lack infinite buses and have low inertia, resulting in higher sensitivity to disturbances and reduced stability compared to grid-tied systems. Enhancing the resilience of IDIMGs can be achieved by maximizing the system loadability and/or mitigating the expected disturbances such as line switching operations. This paper proposes a two-stage framework based on the deployment of mobile energy storage (MES) to enhance the resilience of IDIMGs. In the first stage, the network configuration and deployment of MES are optimized to maximize the system loadability. The proposed formulation for this stage is a stochastic multi-period mixed-integer nonlinear program (MINLP) that maximizes a weighted sum of minimax loadabilities. In the second stage, transitional locations of MES, line-exchange execution sequence, and droop control of dispatchable sources are jointly optimized to mitigate line-switching disturbances that occur when transitioning to the new network configuration obtained in the first stage. The second stage model is a multi-objective MINLP. The proposed models are solved within the general algebraic modeling system (GAMS), utilizing a modified IEEE 33-bus system. Simulations are conducted to assess the significance of each proposed model, and the results reveal remarkable improvements in system loadability with the utilization of the first-stage model and significant reductions in the total switched power with the adoption of the second-stage model.**

***Index Terms*—Droop control, isolated microgrids, minimax loadability, mobile energy storage, smooth reconfiguration.**

NOMENCLATURE

A. Indices and Sets

b	index for MES systems
d	index for representative daily profiles
f	index for intended line-exchange operations
i, j, ii, jj	indices for system buses
$i-j$	index for system lines or transition between buses i and j
k	index for line-exchange execution stages
L^{ex}	set of exchanged lines
ν	index for optimization iterations.
P_r	set of lines in ear r
$\lvert P_r \rvert$	the number of edges that form ear r
r	index for system ears
t	index for time periods

B. Notation

x^{c}	variable/parameter x related to a charging process
x^{d}	variable/parameter x related to a discharging process
x^{g}	variable/parameter x related to a dispatchable source
$x^{\mathrm{g}*}$	reference set value for a variable x related to a dispatchable source
x^{MES}	variable/parameter x related to an MES system
$x^{\min}, x^{\max}$	minimum and maximum values for variable x

Received: September 3, 2024
Accepted: February 20, 2025
Published Online: July 1, 2025

Wael El-sayed (corresponding author) is with the Shoubra Faculty of Engineering, Cairo 11629, Egypt (e-mail: wael.alsayed@feng.bu.edu.eg).

Ahmed Awad is with the Department of Electrical and Computer Engineering, University of Windsor, Windsor N9B 3P4, Canada (e-mail: aawad@uwindsor.ca).

Maher Azzouz is with the Electrical Engineering Department, Qatar University, Doha 2713, Qatar (e-mail: mazzouz@qu.edu.qa).

Mostafa Shaaban is with the Energy, Water and Sustainable Environment Research Center, American University of Sharjah, Sharjah 27272, UAE (e-mail: mshaaban@aus.edu).

Ehab El-Saadany is with the Advanced Power and Energy Center, EE Department, Khalifa University, Abu Dhabi 127788, UAE (e-mail: ehab.elsadaany@ku.ac.ae).

DOI: 10.23919/PCMP.2024.000214

x^{L} variable/parameter x related to a system load
x^{PV} variable/parameter x of a PV source
x^{W} variable/parameter x of a wind source

C. Parameters

C^{FC} ($/km) fuel cost for an MES system
C^{lc} ($/hour) labor cost for operating an MES system
∂ travel distance between two buses
η charging/discharging efficiency for an MES system
K parameter for specifying limits on power factor
M large disjunctive constant
N^{MES} total number of MES systems
R, X resistance and reactance of a line in per unit
ρ probability
T^{lb} time dedicated for a line-exchange stage and MES
W weighting coefficient for modeling multi-objective function

D. Variables

C^{transit} ($) cost of an MES transition for a line-exchange stage
$C^{\mathrm{T,transit}}$ ($) total transition cost of MES systems
$\tilde{\lambda}$ temporal minimax loadability (fraction of nominal load)
λ maximum loadability (fraction of nominal load)
m active power slope for droop control
n reactive power slope for droop control
N^{transit} number of transitions achieved by an MES system
ω angular frequency in per unit
P, Q, S active, reactive, and apparent power in per unit
e_{SOC} state of charge for an MES system
$S^{\mathrm{T,sw}}$ total switched power for exchanged lines in per unit
V, I magnitude of voltage and current of each bus in per unit

E. Binary Variables

δ status of a line, where 1 indicates a closed line
γ auxiliary variable for determining the line-exchange execution sequence
φ transition status of an MES between two buses, where 1 indicates a transition event
Z the connectivity status of an MES system to a bus, where 1 indicates connected

I. Introduction

A. Background and Literature Survey

Isolated microgrids (IMGs) are typically established to supply remote and isolated communities, including rural areas, industrial activities, military bases, aircraft, and ports [1]–[4]. For example, Canada has approximately 300 remote communities in its northern regions, which are not connected to the national grid [1]. Connecting these IMGs to the national grid is uneconomical due to their size and geographic separation. In addition, microgrids with a grid connection may be intentionally islanded due to maintenance or economic reasons [2], [3]. Under specific circumstances, islanded microgrids exhibit similarities to IMGs [4], [5]. As renewable energy resource penetration increases, isolated/islanded microgrids undergo a transition towards inverter-dominated systems, referred to as inverter-dominated isolated/islanded microgrids (IDIMGs) [6], [7].

IDIMGs are characterized by small inertia and low stiffness compared to the main grid due to the lack of infinite bus and bulk synchronous machines. Typical disturbances in grid-tied systems, such as a line or distributed generator (DG) outage, or a line-switching process, could significantly affect the stability and reliability of IDIMGs. Thus, boosting the ability of IDIMGs to withstand disturbances increases their resilience.

To improve the resilience of IDIMGs, one approach is to enhance their load capacity or loadability, which entails increasing the maximum load that the system can handle without exceeding operational limits and constraints [8], [9]. By maximizing loadability, the system's ability to withstand disturbances without experiencing voltage collapse is enhanced. The concept of loadability has been extensively studied and incorporated into power system planning and operational studies [10], [11]. Maximizing the loadability of islanded microgrids is proposed in [12] and [13]. In [12], the effect of droop parameter settings for dispatchable sources (DSs) on the loadability of islanded microgrids is investigated, while in [13], a dynamic power routing scheme is proposed to maximize the loadability of islanded microgrids.

Enhancing the system loadability can also be achieved by optimizing the network configuration. The presence of tie lines in the system is essential for network reconfiguration to maximize the restored loads during faults. During normal operation and considering the existing tie lines, finding the optimal network configuration can be accomplished by considering several objectives such as minimizing the annual system losses [14], increasing the hosting capacity of the system [15], and enhancing the voltage profile [16]. For IDIMGs, the objective of maximizing the system loadability is of prominent importance due to the lack of voltage stiffness.

Mathematical models for determining the optimal

network configuration that maximizes system loadability are proposed in [17] and [18]. In [17], the focus is on conventional distribution networks without the inclusion of distributed generators. The exploration of optimal network configurations and droop settings for DSs to amplify the loadability of islanded microgrids gain traction in [18]. However, the influence of energy storage devices on maximum loadability remains a notable gap.

The incorporation of energy storage devices stands as a potent catalyst for improving system loadability, primarily by reducing peak loads. This pivotal factor affects both optimal network configuration and the maximum loadability of the system. Furthermore, the presence of energy storage devices introduces a time coupling between successive intervals. This interdependence necessitates a departure from the single-period formulation adopted in [18], compelling the adoption of a multi-period framework to effectively encapsulate their operation.

Energy storage devices can be either stationary or mobile. Mobile energy storage (MES) offers spatiotemporal flexibility, which can provide better solutions to system challenges compared to stationary energy storage. MES systems have been shown to provide effective solutions for load restoration through microgrid formation [19]–[22], which may be solely sufficient to economically justify their presence in future power systems. Therefore, MES systems are considered in this paper. The optimal location of energy storage may no longer be optimal when the network configuration changes. As a result, the coordination between network reconfiguration and MES deployment is required while maximizing the network loadability. To this end, a new mathematical formulation that is capable of jointly optimizing the network configuration and MES deployment to maximize the loadability of IDIMGs is required.

Changing the network configuration in IDIMGs poses a significant challenge due to the need for executing a set of line-switching operations in a low-inertia system with non-stiff bus voltages, as discussed in [23] and [24]. While solving the network reconfiguration problem for grid-tied systems, the line-switching operations are either penalized in the objective function using a switching cost term, as in [25] and [26], or constrained to a limited number within the constraints set, as in [27] and [28]. In low-inertia IDIMGs, reducing the number of line-switching operations is insufficient to avoid their detrimental effects, as these operations cause more significant disturbances than in grid-tied systems. These disturbances, in IDIMGs, could cause stability, reliability, and power quality issues in addition to the high wear and tear costs of the switching devices [23]. A superior solution is to find a mechanism for achieving seamless network reconfiguration. Seamless line switching can be realized if the power flow in the switched line is minimized. Consequently, transitional droop control setting is proposed in [23] to minimize the power flow in the lines subject to switching operations. However, if the number of DSs is small in the system, the DSs' ability to minimize the power flow in the switched lines is limited. Furthermore, reference [23] does not consider the utilization of energy storage devices, such as MES systems, to minimize power flow in switched lines. Given their spatiotemporal flexibility, MES systems can offer an effective solution for minimizing power flow in lines undergoing switching operations, with a high probability of achieving zero power flow.

B. Research Gaps and Contributions

To the best of the authors' knowledge, no previous work has proposed a two-fold coordination between seamless network reconfiguration and the deployment of MES systems to enhance the resilience of IDIMGs. Specifically, no research has explored the coordination between network reconfiguration and MES deployment for maximizing the loadability of IDIMGs.

Additionally, prior studies have not considered the use of MES systems to minimize power flow in switched lines for achieving seamless reconfiguration. To address the aforementioned gaps in the literature, this paper aims to enhance the resilience of low-inertia IDIMGs by a two-fold coordination between network reconfiguration and MES deployment. The paper contributes the following to the literature.

1) A mathematical model to jointly determine the optimal network configuration and MES deployment, which maximizes the loadability of IDIMGs.

2) A mathematical model to simultaneously determine the optimal transitional locations of MES systems, line-exchange execution sequence, and transitional droops for DSs in order to minimize the power flow in switched lines for executing seamless network reconfiguration.

3) A two-stage framework that integrates the aforementioned mathematical models to enhance the resilience of IDIMGs while considering the cost of MES transitions.

Enhancing loadability and mitigating line-switching transients contribute to improving the resilience of low-inertia IDIMGs [29]. Both the enhancement in loadability and the reduction in total switched power are quantified and used to assess the improvement in resilience [29], [30].

The rest of the paper is organized as follows. The proposed two-stage framework is introduced in Section II, whereas the mathematical models for the two stages are presented in Sections III and IV, respectively. Section V investigates the effectiveness of the proposed framework, and finally, conclusions are stated in Section VI.

II. Proposed Two-stage Framework

Enhancing the resilience of IDIMGs can be achieved

by strengthening the system and mitigating expected disturbances. One way to harden the system against disturbances that may lead to voltage collapse or nuisance tripping is to increase the system loadability. To achieve this, a two-stage framework is proposed that maximizes the loadability of IDIMGs using a smooth network reconfiguration and MES deployment. The network reconfiguration needs to be seamless in order to minimize disturbances accompanying the line-switching operations required for the reconfiguration process in low-inertia IDIMGs.

Figure 1 illustrates the proposed two-stage framework.

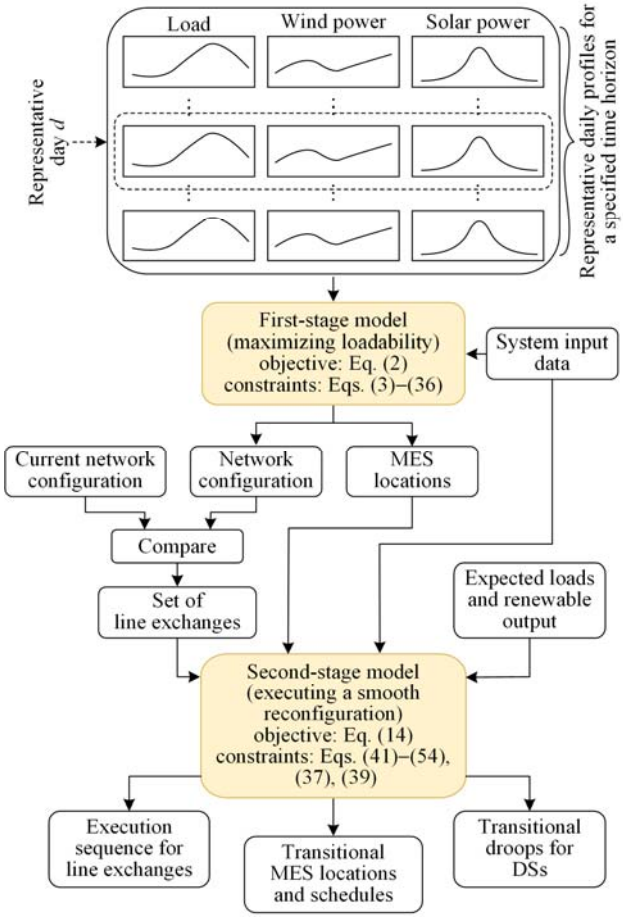

Fig. 1. Proposed framework for resilience enhancement of IDIMGs based on maximizing the loadability using MES and smooth network reconfiguration.

The first stage aims to find the optimal network configuration and MES deployment, which maximize the system loadability for a predefined time horizon, while the second stage aims at mitigating the line-switching transients accompanying the network reconfiguration required by the first stage, i.e., executing a smooth reconfiguration. In the first stage, a stochastic multiperiod formulation is developed to account for the variability and uncertainty of loads and renewable generations, as well as the energy coupling between subsequent time periods due to the existence of MES. The output of the first stage is a single network configuration with fixed locations for the MES systems, tailored to accommodate a predefined array of daily profiles spanning the foreseen time horizon. This fixed output serves to minimize the transportation cost of MES, while concurrently maximizing the system loadability for the considered time horizon.

To change the network configuration to the one obtained in the first stage without introducing significant disturbances to the system, a seamless reconfiguration plan is developed by the second stage of the proposed framework. In the second stage, a multi-objective formulation is proposed. The main objective is to minimize the power flow in the lines subject to line-switching operations to reduce switching transients and achieve a smooth reconfiguration. The second-stage problem is formulated as a multi-objective problem because the cost of MES transitions is modeled as a conflicting objective. The second-stage model provides an optimal routing plan that specifies the transitional locations for the MES systems as they move from their initial locations in the current network to the new positions in the final reconfigured network, as shown in Fig. 2. In these transitional locations, charging and discharging powers are coordinated with the DSs' control to minimize the power flow in specific lines undergoing line-switching operations, such as line *i*–*j*, as demonstrated in Fig. 3. The order of switching these specific lines to achieve the required network reconfiguration, is also determined by the second-stage model. Thus, the second-stage model simultaneously optimizes the execution sequence of line-switching, the transitional droops of DSs, and the transitional locations for MES systems to achieve a smooth reconfiguration. The details on the utilization of transitional droops in DSs and the execution sequence for line switching, have been introduced and explained in [23], though there is no coordination with the employment of MES in [23].

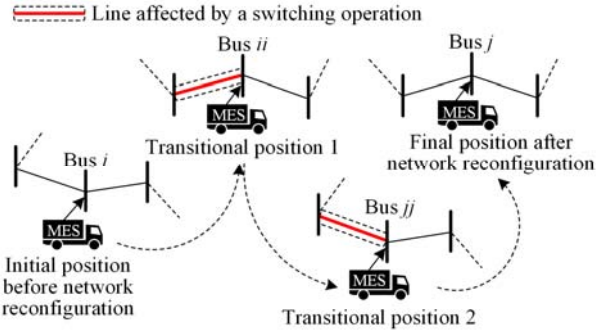

Fig. 2. Utilizing transitional positions of MES systems to minimize the power flow in specific lines for achieving smooth reconfiguration.

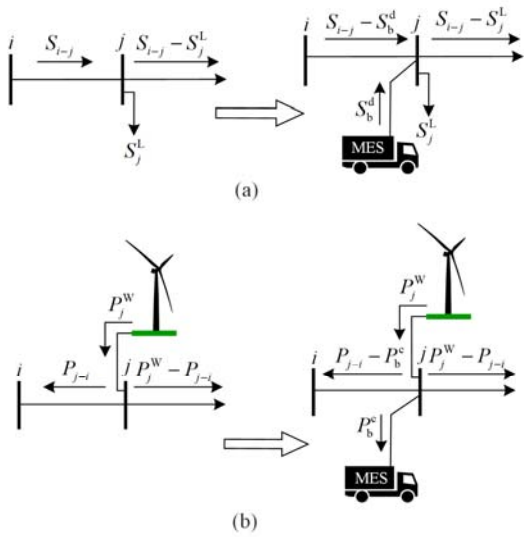

Fig. 3. Examples for power flow reduction in line *i–j* using an MES system. (a) Discharging. (b) Charging.

III. First-Stage Mathematical Model

This section presents the mathematical formulation for the first-stage problem, which involves a stochastic multiperiod network reconfiguration that considers the MES deployment for loadability maximization. The optimization model presented in this section is designated as M1.

A. Objective Function

As the system loading exceeds certain limits, satisfying the power flow constraints becomes infeasible. Increasing the maximum loadability enhances the system's ability to safely ride through generation or line-outage events. Since IDIMGs have limited numbers of DSs without an infinite bus, the maximum loadability of an IDIMG is a critical factor for improving its resilience. Consequently, the selected objective in the first stage is to maximize the system loadability. This objective can be modeled by multiplying the system load with a scaling factor while setting the maximization of this factor as an objective function. However, in the presence of energy storage and renewable generation, the maximum loadability of the system is influenced by the available renewable generation and MES schedule. The presence of MES in the system introduces a complex interplay between time and energy, where optimizing the system's loadability within a specific time period may necessitate compromising loadability during another time period. Therefore, achieving maximum system loadability requires simultaneous optimization across all pertinent time periods under consideration. This objective can be attained by defining the following term:

$$\tilde{\lambda}_d = \min_t \lambda_{d,t} \tag{1}$$

where $\tilde{\lambda}_d$ denotes the temporal minimax loadability (TMML) for day d, which is different from the spatial minimax loadability in [8]; $\lambda_{d,t}$ is the maximum loadability of the system during time period t while considering daily load, wind power, and solar power profiles representative for day d. Maximizing the value of $\tilde{\lambda}_d$, which is equal to the minimum value of $\lambda_{d,t}$, implies optimizing the system loadability for all the considered periods. The concept of maximizing the TMML value is illustrated in Fig. 4 considering only six time periods and four optimization iterations for simplicity, where v is an index for optimization iterations.

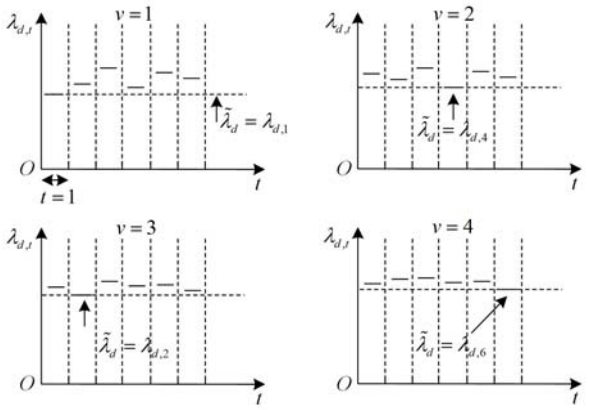

Fig. 4. Illustrating the concept of maximizing the loadability, for a system containing energy storage, by maximizing the temporal minimax loadability.

The final objective function of the proposed model is expressed as follows:

$$\max \sum_d \tilde{\lambda}_d \times \rho_d \tag{2}$$

where ρ_d is the probability of representative day d. Considering several representative days for a certain time horizon such as a season, the proposed model aims to find the optimal network configuration and MES locations that maximize the summation of the minimax loadabilities weighted by the probability of their occurrence.

B. Constraints

The objective function presented in the previous subsection is subject to the following constraints:

$$P^2_{i-j,t,d} + Q^2_{i-j,t,d} = I^2_{i-j,t,d} V^2_{i,t,d}, \ \forall i-j,t,d \tag{3}$$

$$P_{i-j,t,d} + P_{j-i,t,d} = I^2_{i-j,t,d} R_{i-j}, \ \forall i-j,t,d \tag{4}$$

$$Q_{i-j,t,d} + Q_{j-i,t,d} = I^2_{i-j,t,d} X_{i-j}, \ \forall i-j,t,d \tag{5}$$

$$P^{\mathrm{g}}_{i,t,d} + P^{\mathrm{W}}_{i,t,d} + P^{\mathrm{PV}}_{i,t,d} + P^{\mathrm{MES}}_{i,t,d} - \tilde{\lambda}_d \times P^{l}_{i,t,d} = \sum_j P_{i-j,t,d}, \ \forall i,t,d \tag{6}$$

$$Q^{\mathrm{g}}_{i,t,d} + Q^{\mathrm{W}}_{i,t,d} + Q^{\mathrm{PV}}_{i,t,d} + Q^{\mathrm{MES}}_{i,t,d} - \tilde{\lambda}_d \times Q^{l}_{i,t,d} = \sum_j Q_{i-j,t,d}, \ \forall i,t,d \tag{7}$$

$$V_{j,t,d}^2 - V_{i,t,d}^2 + 2(P_{i-j,t,d}R_{i-j} + Q_{i-j,t,d}X_{i-j}) - I_{i-j,t,d}^2(R_{i-j}^2 + X_{i-j}^2) \leqslant (1-\delta_{i-j})M, \ \ \forall i-j,t,d \tag{8}$$

$$V_{j,t,d}^2 - V_{i,t,d}^2 + 2(P_{i-j,t,d}R_{i-j} + Q_{i-j,t,d}X_{i-j}) - I_{i-j,t,d}^2(R_{i-j}^2 + X_{i-j}^2) \geqslant (\delta_{i-j}-1)M, \ \ \forall i-j,t,d \tag{9}$$

$$P_{i-j,t,d}^2 + Q_{i-j,t,d}^2 \leqslant \delta_{i-j}(S_{i-j}^{\max})^2, \ \ \forall i-j,t,d \tag{10}$$

$$(P_{i,t,d}^{\mathrm{g}})^2 + (Q_{i,t,d}^{\mathrm{g}})^2 \leqslant (S_i^{\mathrm{g,max}})^2, \ \ \forall i,t,d \tag{11}$$

$$P_i^{\mathrm{g,min}} \leqslant P_{i,t,d}^{\mathrm{g}}, \ \ \forall i,t,d \tag{12}$$

$$Q_i^{\mathrm{g,min}} \leqslant Q_{i,t,d}^{\mathrm{g}}, \ \ \forall i,t,d \tag{13}$$

$$V^{\min} \leqslant V_{i,t,d} \leqslant V^{\max}, \ \ \forall i,t,d \tag{14}$$

$$\omega = \omega_{i,t,d}^{\mathrm{g}^*} - m_{i,t,d}^{\mathrm{g}} P_{i,t,d}^{\mathrm{g}}, \ \ \forall i,t,d \tag{15}$$

$$V_{i,t,d} = V_{i,t,d}^{\mathrm{g}^*} - n_{i,t,d}^{\mathrm{g}} Q_{i,t,d}^{\mathrm{g}}, \ \ \forall i,t,d \tag{16}$$

$$\omega^{*\min} \leqslant \omega_{i,t,d}^{\mathrm{g}^*} \leqslant \omega^{*\max}, \ \ \forall i,t,d \tag{17}$$

$$V^{*\min} \leqslant V_{i,t,d}^{\mathrm{g}^*} \leqslant V^{*\max}, \ \ \forall i,t,d \tag{18}$$

$$m^{\min} \leqslant m_{i,t,d}^{\mathrm{g}} \leqslant m^{\max}, \ \ \forall i,t,d \tag{19}$$

$$n^{\min} \leqslant n_{i,t,d}^{\mathrm{g}} \leqslant n^{\max}, \ \ \forall i,t,d \tag{20}$$

$$\sum_i \sum_b Z_{i,b} = N^{\mathrm{MES}} \tag{21}$$

$$\sum_i Z_{i,b} = 1, \ \ \forall b \tag{22}$$

$$0 \leqslant P_{b,t,d}^{c} \leqslant P_b^{c,max}, \ \ \forall b,t,d \tag{23}$$

$$0 \leqslant P_{b,t,d}^{d} \leqslant P_b^{d,max}, \ \ \forall b,t,d \tag{24}$$

$$P_{i,t,d}^{\mathrm{MES}} = \sum_b Z_{i,b} \times (P_{b,t,d}^{d} - P_{b,t,d}^{c}), \ \ \forall i,t,d \tag{25}$$

$$e_{\mathrm{SOC},b,t,d} = e_{\mathrm{SOC},b,t-1,d} + \left(\eta_b^c P_{b,t,d}^c - \frac{P_{b,t,d}^d}{\eta_b^d} \right) \Delta t \tag{26}$$

$$e_{\mathrm{soc},b}^{\min} \leqslant e_{\mathrm{soc},b,t,d} \leqslant e_{\mathrm{soc},b}^{\max}, \ \ \forall b,t,d \tag{27}$$

$$\sum_t \left(\eta_b^c P_{b,t,d}^c - \frac{P_{b,t,d}^d}{\eta_b^d} \right) = 0, \quad \forall b,d \tag{28}$$

$$(P_{b,t,d}^d)^2 + (Q_{b,t,d}^d)^2 \leqslant (S_b^{\mathrm{MES,max}})^2, \ \ \forall b,t,d \tag{29}$$

$$Q_{b,t,d}^d \leqslant P_{b,t,d}^d \times K^{\mathrm{MES}}, \ \ \forall b,t,d \tag{30}$$

$$Q_{i,t,d}^{\mathrm{MES}} = \sum_b Z_{i,b} \times Q_{b,t,d}^d, \ \ \forall i,t,d \tag{31}$$

$$Q_{i,t,d}^{\mathrm{W}} \leqslant P_{i,t,d}^{\mathrm{W}} \times K^{\mathrm{W}}, \ \ \forall i,t,d \tag{32}$$

$$Q_{i,t,d}^{\mathrm{PV}} \leqslant P_{i,t,d}^{\mathrm{PV}} \times K^{\mathrm{PV}}, \ \ \forall i,t,d \tag{33}$$

$$(P_{i,t,d}^{\mathrm{W}})^2 + (Q_{i,t,d}^{\mathrm{W}})^2 \leqslant (S_i^{\mathrm{W,max}})^2, \ \ \forall i,t,d \tag{34}$$

$$(P_{i,t,d}^{\mathrm{PV}})^2 + (Q_{i,t,d}^{\mathrm{PV}})^2 \leqslant (S_i^{\mathrm{PV,max}})^2, \ \ \forall i,t,d \tag{35}$$

$$\sum_{i-j \in P_r} \delta_{i-j} = |P_r| - 1, \ \ \forall r \tag{36}$$

The power flow and power balance constraints are modeled by (3)–(9). In (6) and (7), the active and reactive power loads are scaled with $\tilde{\lambda}_d$, which is maximized by (2). Equation (10) expresses the upper limit on the line flow, while constraints (11)–(13) represent the upper and lower limits on the active and reactive output power from the DSs. Constraint (14) limits the bus voltage within a certain range, while equations (15)–(16) express the droop control for the DSs. The upper and lower limits on the variables of the droop control are specified by (17)–(20), equations (21)–(31) model the MES system and limit its output power, whereas constraint (32)–(35) present the upper and lower limits on the output power from the renewable sources. Finally, equation (36) forces the radiality structure of the system. More information on preserving the system radiality through the ear decomposition of the network graph can be found in [8].

IV. Second-stage Mathematical Model

The objective of the second stage is to smoothly change the current network configuration to the one obtained in the first stage. The network reconfiguration process requires the execution of a set of line-opening and line-closing operations. However, in a radial network, opening a single line divides the system into two islands, potentially leaving some system nodes without supply. Conversely, closing an additional line converts the radial structure into a weakly meshed one, potentially disrupting the operation of protection devices designed for radial networks. To maintain a single island with a radial structure during network reconfiguration, line-exchange operations are executed. A line-exchange operation involves two associated line-switching operations: one line-opening and one line-closing operation. Therefore, any network reconfiguration process for a radial network can be defined by a set of line-exchanges to be executed.

A. Modeling Line-exchange Execution Sequence

Executing a certain line-exchange operation changes the network configuration and affects the power flow in the lines subject to subsequent line-exchange operations. The main concern is the increase in the power flow in those lines as the result of this change. Consequently, there is a need to determine the optimal line-exchange execution sequence that minimizes the total switched power in the lines subject to line-exchange operations. To model a line-exchange sequence, let L^{ex} denotes the set of line-exchange operations required to change the network configuration and let f be the index for line-exchange operations in L^{ex}. In L^{ex}, each line-exchange operation is represented by $\left(\widetilde{i-j}, \widehat{i-j}\right)$, where $\widetilde{i-j}$ indicates the line subjected to a line-opening operation and $\widehat{i-j}$ points to the line subjected to the associated line-closing operation. To

determine the execution sequence of the line-exchange operations identified in L^{ex} let k be the index for the line-exchange execution stages. Thereafter, binary variable $\gamma_{k,f}$ is introduced to determine which intended line-exchange indexed by f will be executed at which execution stage, indexed by k. Table I gives an example of an execution sequence for a set of three intended line-exchange operations. The three assumed operations for the purpose of illustration are $L^{\text{ex}} = \left\{(\widetilde{8-9}, \widehat{12-22}),\ (\widetilde{23-24}, \widehat{25-29}),\ (\widetilde{31-32}, \widehat{18-33})\right\}$. According to the values of $\gamma_{k,f}$ in Table I, the execution sequence is L_2^{ex}, L_3^{ex}, then L_1^{ex}. The optimization model, designated as M2, for the second-stage problem is detailed in the following subsections, based on the modeling approach for the line-exchange execution sequence presented in this subsection.

TABLE I
EXAMPLE OF A LINE-EXCHANGE EXECUTION SEQUENCE DETERMINED BY $\gamma_{k,f}$

	$f=1$ $(\widetilde{8-9}, \widehat{12-22})$	$f=2$ $(\widetilde{23-24}, \widehat{25-29})$	$f=3$ $(\widetilde{31-32}, \widehat{18-33})$
$k=1$	$\gamma_{1,1}=0$	$\gamma_{1,2}=1$	$\gamma_{1,3}=0$
$k=2$	$\gamma_{2,1}=0$	$\gamma_{2,2}=0$	$\gamma_{2,3}=1$
$k=3$	$\gamma_{3,1}=1$	$\gamma_{3,2}=0$	$\gamma_{3,3}=0$

B. Objective Function

The main objective of the second stage is to execute a smooth network reconfiguration in low-inertia IDIMGs. This objective can be achieved by minimizing the power flow in lines subjected to line-switching operations. To accomplish this minimization, the line-opening operation is weighted by $S_{\widetilde{i-j}}$, and the line-closing operation is weighted by $S_{\widehat{i-j}}$, where $S_{\widetilde{i-j}}$ represents the apparent power flow in line $\widetilde{i-j}$ immediately before executing the line-opening operation and $S_{\widehat{i-j}}$ represents the apparent power flow in line $\widehat{i-j}$ once the line is closed. Thereafter, the total switched power can be evaluated by:

$$S^{\text{T,sw}} = \sum_k \sum_f \gamma_{k,f} \times \left(\left(S_{\widetilde{i-j},k}\right)^2 + \left(S_{\widehat{i-j},k}\right)^2 \right) \tag{37}$$

The main objective of the second-stage model is to minimize $S^{\text{T,sw}}$ to achieve a smooth network reconfiguration in IDIMGs. This objective is achieved by simultaneously optimizing the transitional droops of the DSs, the line-exchange execution sequence, and the transitional positions of the MES systems. However, the IDIMG operator may prioritize minimizing the cost associated with transitioning the MES while also minimizing $S^{\text{T,sw}}$. This cost can arise from the additional movement of the MES systems to minimize the power flow in the exchanged lines, and can be expressed as:

$$C_{b,k}^{\text{transit}} = C^{\text{FC}} \times \varphi_{i-j,b,k} \times \partial_{i-j} + C^{\text{lc}} \times T_{b,k}^{\text{lb}} \tag{38}$$

where $C_{b,k}^{\text{transit}}$ is the cost of moving MES b during line-exchange stage k; $\varphi_{i-j,b,k}$ is an auxiliary variable to indicate the transition status of MES b during line-exchange stage k between buses i and j; ∂_{i-j} stands for the distance between buses i and j; and $T_{b,k}^{\text{lb}}$ is the time dedicated for each line-exchange stage and MES b. The total transition cost for all MES systems is $C^{\text{T,transit}}$, given by:

$$C^{\text{T,transit}} = \sum_b \sum_k C_{b,k}^{\text{transit}} \tag{39}$$

It is required to minimize $C^{\text{T,transit}}$ while also minimizing the total switched apparent power. Since these two objectives are conflicting, the problem is formulated as a multi-objective optimization problem, where one of the objectives is weighted by scalar factor W. The final objective function for the second-stage model can be written as:

$$\text{Min}\ (S^{\text{T,sw}} + WC^{\text{T,transit}}) \tag{40}$$

It is worth noting that minimizing (40) for different values of W offers a set of Pareto-optimal solutions to the system operator.

C. Constraints

The objective function presented in the previous subsection is subject to the following constraints:

$$(3)-(5),\ (8)-(9),(10),\ \forall i-j,k \tag{41}$$

$$(6)-(7),\ (11)-(13),\ (14),\ (15)-(16),\ (17)-(20),\ (25),\ (31),\ (32)-(35),\ \forall i,k \tag{42}$$

$$(21),\ \forall k \tag{43}$$

$$(22)-(24),\ (29)-(30),\ \forall b,k \tag{44}$$

$$\sum_{i-j} \delta_{i-j,k} = 1 + \sum_r \left(|P_r| - 1\right),\ \forall k \tag{45}$$

$$\delta_{\widetilde{i-j},k} \leqslant \delta_{\widetilde{i-j},k-1},\ \forall k \geqslant 1, \forall \widetilde{i-j} \in L^{\text{ex}} \tag{46}$$

$$\delta_{\widetilde{i-j},k} + \delta_{\widehat{i-j},k} = \gamma_{k,f} + 1,\ \forall k, \forall \left(\widetilde{i-j}, \widehat{i-j}\right) \in L^{\text{ex}} \tag{47}$$

$$\sum_k \gamma_{k,f} = 1,\ \forall f \tag{48}$$

$$\sum_{\widetilde{i-j}} \delta_{\widetilde{i-j},k} = \sum_{\widetilde{i-j}} \delta_{\widetilde{i-j},k-1} - 1,\ \forall k \geqslant 1 \tag{49}$$

$$\delta_{i-j,k} = \delta_{i-j,0},\ \forall k \geqslant 1, \forall (i-j) \notin L^{\text{ex}} \tag{50}$$

$$\varphi_{i-j,b,k} = Z_{i,b,k-1} \times Z_{j,b,k},\ \forall i \neq j, k \geqslant 1, b \tag{51}$$

$$C_{b,k}^{\text{transit}} = C^{\text{FC}} \times \varphi_{i-j,b,k} \times \partial_{i-j} + C^{\text{lc}} \times T_{b,k}^{\text{lb}},\ \forall b,k \tag{52}$$

$$\left(S_{\widetilde{i-j},k}\right)^2 = \left(P_{\widetilde{i-j},k}\right)^2 + \left(Q_{\widetilde{i-j},k}\right)^2,\ \forall k \geqslant 1, \forall \widetilde{i-j} \in L^{\text{ex}} \tag{53}$$

$$\left(S_{\widehat{i-j},k}\right)^2=\left(P_{\widehat{i-j},k}\right)^2+\left(Q_{\widehat{i-j},k}\right)^2, \quad \forall k \geqslant 1, \forall \widehat{i-j} \in L^{\mathrm{ex}} \text{ and (37), (39)} \tag{54}$$

Equations (41)–(44) aggregate the same constraints in M1, but for different indices. In (41)–(44), the variables are $P_{i-j,k}$, $P_{j-i,k}$, $Q_{i-j,k}$, $Q_{j-i,k}$, $I_{i-j,k}$, $V_{i,k}$, $P_{i,k}^{\mathrm{g}}$, $P_{i,k}^{\mathrm{MES}}$, $Q_{i,k}^{\mathrm{g}}$, $Q_{i,k}^{\mathrm{MES}}$, $\delta_{i-j,k}$, ω, $m_{i,k}^{\mathrm{g}}$, $n_{i,k}^{\mathrm{g}}$, $\omega_{i,k}^{\mathrm{g}*}$, $V_{i,k}^{\mathrm{g}*}$, $Z_{i,b,k}$, $P_{b,k}^{\mathrm{c}}$, and $P_{b,k}^{\mathrm{d}}$. Equation (45) specifies the total number of closed lines during each line-exchange stage. If a line is selected to be opened in a specific stage, it will remain open in the following stages due to (46). Equation (47) connects the current line-exchange stage with the status of the associated lines, while equation(48) ensures that one line exchange operation is executed during each stage. Equation (49) ensures that one line is opened in each stage, equation (50) fixes the status of the lines that do not belong to the set L^{ex} during all the line-exchange stages, whereas (51) determines the transition status of MES b during switching stage k between buses i and j based on the connectivity status of the MES. Equations (52)–(54), (37), and (39) compute the variables required for the objective function (40).

V. Results

Several case studies are presented to investigate the effectiveness of the proposed resilience enhancement framework for IDIMGs. The details of these case studies as well as the input data are presented in the following subsections.

A. System and Input Data

The IEEE 33-bus system is considered in this paper. The line data of this system are available in [31], while the rated active and reactive power loads, as well as the residential load, commercial load, wind power, and solar power profiles, are adopted from [32]. The system is modified by adding two DSs at buses 1 and 18, respectively, with each DS rated at 2.8 MVA and a minimum power factor of 0.8. Two wind and two solar power sources are added to the system, located and sized identically to those in [27]. Unity power factors for all renewable sources are assumed. The ratings and bus locations of the dispatchable and renewable sources are presented in Table II, and the modified IEEE 33-bus system is displayed in Fig. 5. As seen in Fig. 5, the assumed system ears are highlighted with different colors, where the ear decomposition approach for preserving the network radiality in [8] is adopted. The analysis focuses on a single MES system rated at 500 kW/776 kWh [21], [33], assuming η_b^{d} and η_b^{c} are both 0.9.

A personal computer with a Core i7 processor (1.99 GHz) and 8 GB of RAM is used for conducting all the optimization. The proposed mixed-integer nonlinear program (MINLP) models are solved in general algebraic modeling system (GAMS) using the SBB solver. This solver aggregates the standard branch and bound (B&B) algorithm for treating the integrity constraints with some standard NLP solvers for solving the relaxed MINLP.

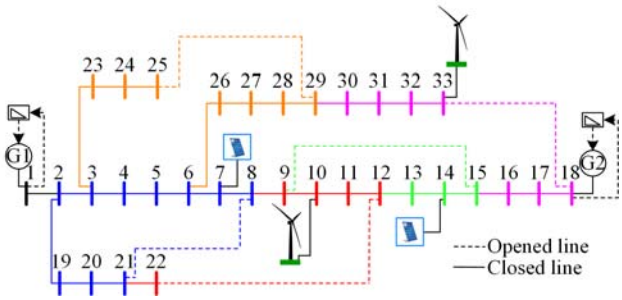

Fig. 5. The modified IEEE 33-bus system.

TABLE II
Locations and Ratings of the DGs

(MVA)

Type	DS1	DS1	Wind1	Wind2	Solar1	Solar2
Rating	2.8	2.8	0.4	0.5	0.35	0.45
Bus number	1	18	10	33	7	14

B. Assessment of the First Stage

The obtained solution from the first-stage model is fixed for a time horizon of one season, using the input data for the winter season obtained from [32]. To represent the season, six representative days are considered, with two days adopted for each month. One day represents weekday profiles, while the other represents weekend profiles. To demonstrate the significance of jointly optimizing network reconfiguration and MES locations while maximizing system loadability, the TMML is evaluated using four different study cases. All of these cases adopt M1, either with or without some modifications, and are denominated as M1-Case1, M1-Case2, M1-Case3, and M1-Case4. The following paragraphs provide details and results for each study case.

1) M1-Case 1

The initial network configuration in [27], [31] shown in Fig. 5 is assumed to be fixed, with the opened lines being 8–21, 12–22, 9–15, 25–29, and 18–33. Additionally, no energy storage is incorporated in the system. To establish M1-Case1, the proposed first-stage model (M1) is modified by adding additional constraints, which force the intended network configuration shown in Fig. 5 to be fixed. Furthermore, to prevent the incorporation of MES, constraints (21) and (22) in M1 are modified.

The purpose of M1-Case1 is to assess the value of the TMML if no energy storage is considered and the network configuration is not optimized for maximizing the TMML. The only decision variables are the droop settings that maximize the loadability of the six-representative days for the winter season. Figure 6 displays the maximum loadability value for each hour

($\lambda_{d,t}$) obtained by M1-Case1 based on optimizing the droop settings only. The obtained TMML value in this case is 0.8975, which is lower than 1 due to the unoptimized network configuration and the absence of energy storage. The effect of optimizing the network configuration and the MES deployment on the TMML is investigated in the following case studies.

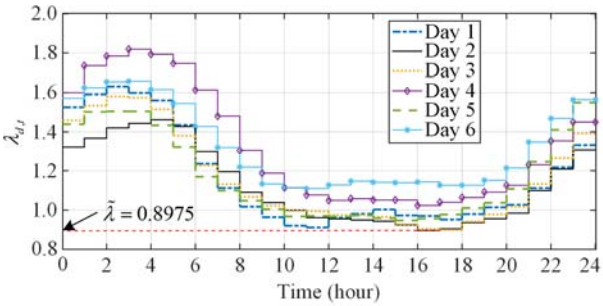

Fig. 6. Maximum hourly loadabilities and TMML value obtained by M1-Case1.

2) M1-Case2

To demonstrate the effect of considering the energy storage on the TMML value, the initial network configuration is considered with one available MES system. Consequently, additional constraints are added to fix the initial configuration shown in Fig. 5, while constraints (21) and (22) remain unchanged in M1. Figure 7 displays the maximum hourly loadabilities obtained by solving M1-Case2. As seen, the worst maximum hourly loadability, i.e., the TMML value, is 0.951, when the MES is located at bus 33. Due to the consideration of a single MES system, the TMML value is improved by 5.63%. In Fig. 7, it can be observed that the loadability curves are flattened due to the maximization of the TMML value while considering energy storage.

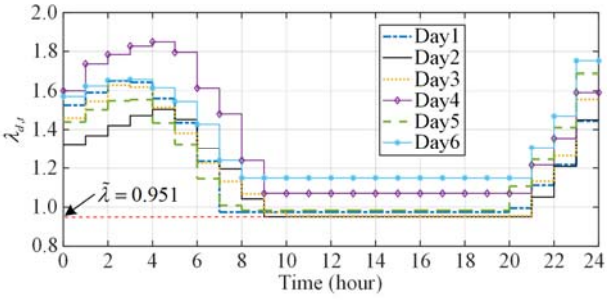

Fig. 7. Maximum hourly loadabilities and TMML value obtained by M1-Case2.

3) M1-Case3

To demonstrate the effect of optimizing the network configuration on the TMML value, the optimal configuration that maximizes the TMML value without using energy storage is considered in this case. This entails modifying only constraints (21) and (22) in M1. Figure 8 plots the maximum hourly loadabilities of the six representative days for the winter season. By comparing Fig. 8 with Fig. 6, it can be observed that all the hourly maximum loadabilities are increased and the TMML value is 1.137, which represents a 21% improvement compared to that of M1-Case 1. The obtained network configuration incorporates opening lines 7–8, 11–12, 13–14, 6–26, and 15–16.

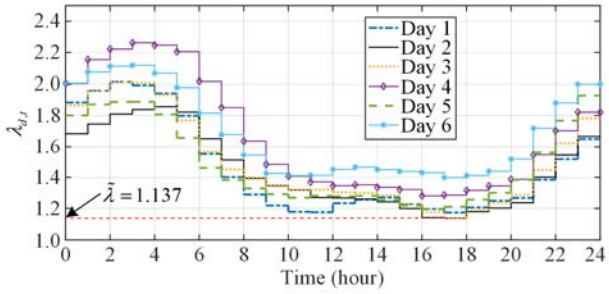

Fig. 8. Maximum hourly loadabilities and TMML value obtained by M1-Case3.

4) M1-Case4

In this case, no modification is added to the proposed model M1. Consequently, joint optimization of the network configuration and MES deployment are attained. Figure 9 displays the maximum hourly loadabilities for the considered representative days. It shows that the maximum hourly loadabilities for all the considered days are improved compared to the previous cases where only the network configuration or MES deployment was optimized. The obtained solution involves opening lines 8–21, 11–12, 14–15, 23–24, and 15–16, and connecting the MES to bus 12, as illustrated in Fig. 10.

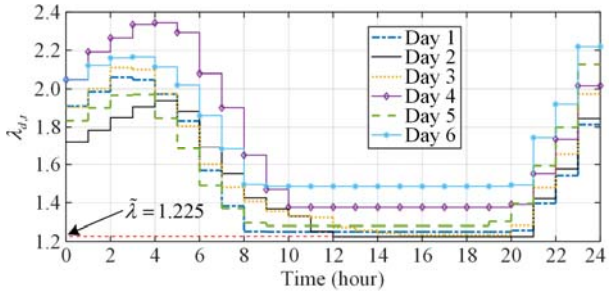

Fig. 9. Maximum hourly loadabilities and TMML value obtained by M1-Case4.

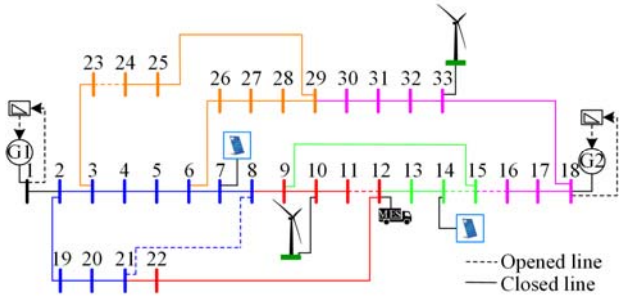

Fig. 10. Network configuration and MES deployment obtained from solving M1 considering the winter season.

The TMML value obtained is 1.225, which exceeds those of M1-Case1, M1-Case2, and M1-Case3 by 26.74%, 22.37%, and 7.18%, respectively.

The following subsection outlines a strategy to achieve a smooth network reconfiguration when transitioning the network from the unoptimized configuration in M1-Case2 to the optimized configuration in M1-Case4. This network reconfiguration is also accompanied by relocating the MES from bus 33 to bus 12.

C. Assessment of the Second Stage

Upon comparing the set of opened lines obtained in M1-Case 4 with those in M1-Case 2, the following set of line exchanges must be executed to reconfigure the network: $L^{\text{ex}} = \left\{\left(\widetilde{11-12},\widetilde{12-22}\right),\left(\widetilde{14-15},\widetilde{9-15}\right),\left(\widetilde{23-24},\widetilde{25-29}\right),\left(\widetilde{15-16},\widetilde{18-33}\right)\right\}$. The cost coefficients used to evaluate the cost of MES transition are $C^{\text{FC}} = 0.4\ \$/\text{km}$ and $C^{\text{lc}} = 25\ \$/\text{hour}$ [34]. The distance between any two adjacent buses is assumed to be 0.5 km. Thereafter, the Euclidean distances between any two non-adjacent buses are computed.

By solving M2, three main decisions are determined: the transitional droop settings, the execution sequence for desired line exchanges, and the transitional locations of MES systems. To investigate the impact of optimizing different decisions on the primary objective of minimizing the total switched power, four case studies are conducted, namely: M2-Case1, M2-Case2, M2-Case3, and M2-Case4. For the four cases, M2 is solved while setting $W = 0$ in (40). This setting implies that the IDIMG operator highly prefers minimizing the switching transients irrespective of the associated costs due to MES transitions. Thereafter, M2-Case5 is developed to assess the effect of considering different values of W on the obtained solution.

1) M2-Case1

The aim of this study case is to assess the total switched power if none of the above-mentioned decisions are optimized for minimizing the total switched power. This aim can be achieved by replacing the objective function in (40) with a different trivial objective, such as minimizing the voltage regulation. The total switched power, in this case, is 1.272 p.u. (1.272 MVA). The line-exchange execution sequence and MES locations that minimize the voltage regulation are shown in Fig. 11. It shows the exchanged lines for each line-exchange stage identified by the index k, while it also indicates the location of the MES and the switched power at each stage. According to Fig. 11, the initial line-exchange process involves opening line 15–16 and closing line 18–33. At this stage, the MES is located at bus 28. As the network configuration changes with each line-exchange operation, the MES changes its location in subsequent stages to minimize the voltage regulation.

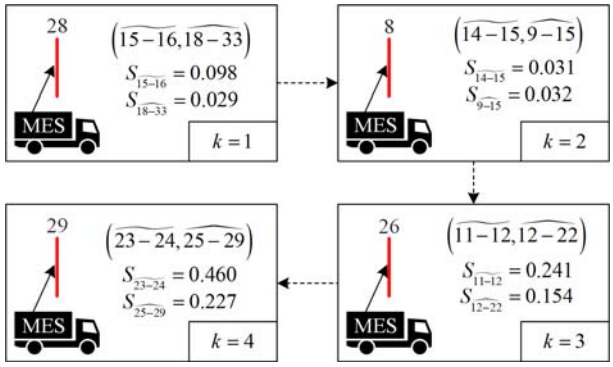

Fig. 11. The line-exchange execution sequence and transitional locations of the MES obtained by solving M2-Case1.

2) M2-Case2

The objective of this case is to investigate the effect of optimizing only the droop control of the DSs on minimizing the total switched power. The order of line-exchange operations and transitional positions, obtained by solving M2-Case1 and depicted in Fig. 11, remains fixed. To establish the study case identified as M2-Case2, additional constraints are added to M2 to enforce the fixed order and positions as indicated by Fig. 11. The total switched power obtained in M2-Case2 is 1.068 p.u., which is 16% lower than the value obtained in M2-Case1. This reduction is a result of optimizing the transitional droops to minimize the total switched power.

3) M2-Case3

This case study evaluates the impact of simultaneously optimizing the droop control of the DSs and the line-exchange execution sequence while maintaining the MES locations as specified by M2-Case1. M2-Case3 is similar to M2-Case2, except that it does not include additional constraints to force a certain line-exchange execution sequence. The total switched power in M2-Case3 is 0.795 p.u., representing a 37.5% reduction compared to M2-Case1 and an improvement of 25.6% compared to M2-Case2 due to the optimized line-exchange execution sequence. The line-exchange execution sequence and transitional locations of the MES obtained by solving M2-Case3 are displayed in Fig. 12.

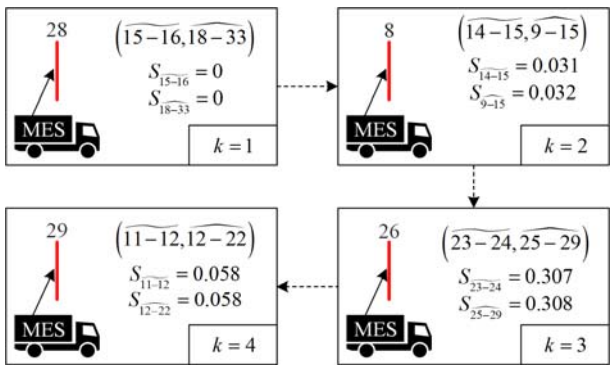

Fig. 12. The line-exchange execution sequence and transitional locations of the MES obtained by solving M2-Case3.

4) M2-Case4

The optimization model M2 is solved without any additional constraints or changes to the objective function, as in the previous cases (M2-Case1, M2-Case2, and M2-Case3). Therefore, the droop settings, line-exchange execution sequence, and transitional MES locations are all simultaneously optimized. The total switched power attained by solving M2, with $W=0$, is 0.140 p.u. This value indicates an 89% reduction in the total switched power compared to the case of non-optimized decisions for minimizing the total switched power, i.e., M2-Case1. The obtained line-exchange execution sequence and the transition plan for the MES are displayed in Fig. 13.

The transition plan in Fig. 13 indicates that instead of moving directly from bus 33 in the initial network configuration to bus 12 in the final network configuration, the MES moves to transitional bus 24 and then bus 11 while moving from bus 33 to bus 12. It should be noted that the total switched power could be reduced to zero if two MES systems were available with the mentioned specifications instead of one, or if the power rating of the single available MES increased to 0.71 p.u. from 0.5 p.u.

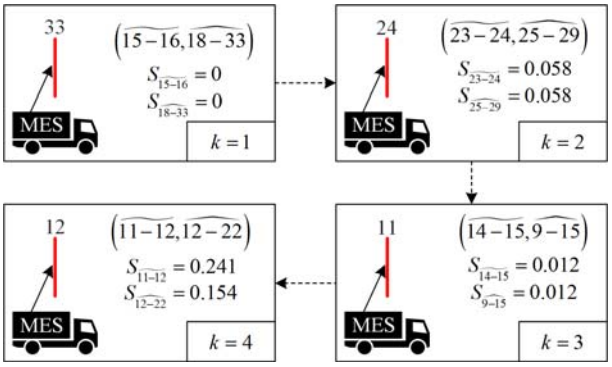

Fig. 13. The line-exchange execution sequence and transitional locations of the MES obtained by solving M2-Case4.

5) M2-Case5

This case aims to evaluate the effect of considering the travel cost of the MES system while minimizing the total switched power. This is achieved by varying the value of *W*, which reflects the different preferences of the system operator. M2 was solved for thirty values of *W* between 0 and 200, though only three non-dominated solutions were obtained, corresponding to the best solutions for one, two, and three transitions of the MES system. Therefore, when $W=0$, the maximum number of transitions is three, whereas as *W* increases towards 200, the number of transitions decreases to two and then to one. Figure 14 displays the values of the two objectives for the three non-dominated solutions, where each non-dominated solution is associated with a value of N^{transit}, representing the number of transitions accomplished by the MES. Using the generated non-dominated solutions, the system operator can select the desired solution based on a techno-economic study for the considered IDIMG. This techno-economic study balances the limits on the system disturbances (the allowed maximum switched power) and the allowed economic budget for moving the MES.

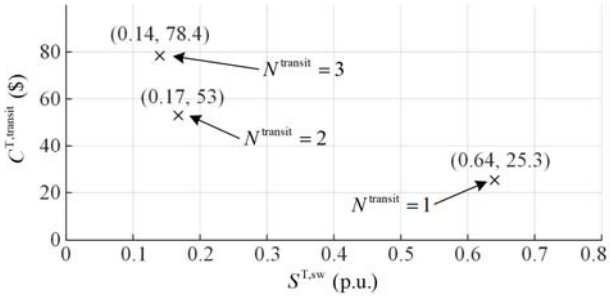

Fig. 14. Values of objective functions for three different non-dominated solutions corresponding to three values of N^{transit}.

VI. Conclusion

This paper proposes a two-stage framework that utilizes mobile energy storage systems to enhance the resilience of inverter-dominated isolated/islanded microgrids. In the first stage, a new mathematical formulation is proposed to maximize the temporal minimax loadability of the inverter-dominated isolated/islanded microgrid based on optimizing the network configuration and the mobile energy deployment. In the second stage, another new mathematical formulation is proposed to minimize the total switched power for smoothly transitioning to the network configuration obtained from the first stage. The decision variables for the second-stage model are the transitional droop settings, the execution sequence for the desired line exchanges, and the transitional locations of the MES systems.

Several case studies have been conducted to investigate the effectiveness of each proposed model. The results of these case studies indicate that jointly optimizing the network configuration and mobile energy storage deployment can result in a 26.7% improvement in temporal minimax loadability. Additionally, when a single mobile energy storage system with a power rating of 0.5 p.u. is used, the reduction in the total switched power ranges from 49% to 89%, depending on the budget allocated for the mobile energy storage transition.

Acknowledgment

Not applicable.

Authors' Contributions

Wael El-Sayed: conceptualization, methodology, formal analysis, validation, simulation, writing original draft, and writing review & editing. Ahmed Awad, Maher Azzouz, Mostafa Shaaban, and Ehab El-Saadany: supervision, project administration, validation, funding

acquisition, and writing review & editing. All authors read and approved the final manuscript.

FUNDING

This work is supported in part by fund No. FRG22-C-E24 and the open access program at the American University of Sharjah. (This paper represents the opinions of the authors and does not mean to represent the position or opinions of the American University of Sharjah.)

AVAILABILITY OF DATA AND MATERIALS

Please contact the corresponding author for data material request.

DECLARATIONS

Competing interests: The authors declare that they have no known competing financial interests or personal relationships that could have appeared to influence the work reported in this article.

AUTHORS' INFORMATION

Wael El-Sayed was born in Qaluobia, Egypt in 1985. He received his B.Sc. (with honors) degree from the Shoubra Faculty of Engineering, Benha University, Egypt in 2007, the M.Sc. degree from the Department of Electrical and Computer Engineering, University of Waterloo, Waterloo, ON, Canada in August 2014, and the Ph.D. degree in electrical engineering from Benha University, Cairo, Egypt, in 2018. From Mar. 2019 till Nov. 2021, he served as a postdoctoral fellow with the Department of Electrical Engineering and Computer Science at Khalifa University, Abu Dhabi, UAE. Since December 2021, he has been affiliated with the Department of Electrical Engineering, Shoubra Faculty of Engineering, Benha University, Egypt. Additionally, he is currently a postdoctoral fellow with the Department of Electrical and Computer Engineering at the University of Windsor, Windsor, ON, Canada. His research interests encompass a wide range of topics, including the economic dispatch problem, applications of decentralized and distributed algorithms in power systems, and the protection of microgrids.

Ahmed Awad received the B.Sc. and the M.Sc. degrees in electrical engineering from Ain Shams University, Cairo, Egypt, in 2007 and 2010, respectively, and the Ph.D. degree from the Electrical and Computer Engineering Department, University of Waterloo, Waterloo, ON, Canada, in 2014. In between 2007 and 2009, he worked as an electrical design engineer with Dar El-Handasah (Shair and partners) and Allied Consultants Co. in Egypt. He also worked with Siemens Canada Limited between 2014 and 2016. He worked with CanmetENERGY, Natural Resources Canada, as a research engineer between 2016 and 2022. He is an adjunct associate professor at the Electrical and Computer Engineering Department, University of Windsor, ON, Canada. His research interests include integration of sustainable energy technologies into power systems, electricity market equilibrium, as well as operation and control of power systems. Dr. Awad is currently an editor for the *IEEE Transactions on Sustainable Energy*, and a registered professional engineer in the Province of Ontario, Canada.

Maher Azzouz received the B.Sc. and M.Sc. degrees (Hons.) in electrical power engineering from Cairo University, Giza, Egypt, in 2008 and 2011, respectively, and the Ph.D. degree in electrical and computer engineering from the University of Waterloo, Waterloo, ON, Canada, in 2016. He was a postdoctoral fellow with the Power and Energy System Group, University of Waterloo. He is currently on leave with the Department of Electrical and Computer Engineering, University of Windsor, Windsor, ON, Canada, and is with the Electrical Engineering Department, Qatar University, Qatar. His research interests include control of power electronic converters, power system protection, distribution system operation and planning, and renewable energy sources. He has been recognized as one of the best reviewers of the *IEEE Transactions on Smart Grid*. Dr. Azzouz is a registered professional engineer in the province of Ontario.

Mostafa Shaaban received the B.Sc. and M.Sc. degrees in electrical engineering from Ain Shams University, Cairo, Egypt, in 2004 and 2008, respectively, and the Ph.D. degree in electrical engineering from the University of Waterloo, Waterloo, ON, Canada, in 2014. Currently, he is the director of Energy, Water and Sustainable Environment Research Center and an associate professor of electrical engineering, American University of Sharjah, Sharjah, United Arab Emirates and adjunct associate professor with University of Waterloo, Waterloo, Canada. He was with Independent Electricity System Operator (IESO) and Opus One Solutions. Dr. Shaaban has several publications in international journals and conferences. He serves as an associate editor for *IET Smart Grid*, and *IET Energy Conversion and Economics*. His research interests include smart grid, renewable DG, distribution system planning, electric vehicles, storage systems, and bulk power system reliability.

Ehab El-Saadany is an IEEE Fellow for his contributions in distributed generation planning, operation and control. He was born in Cairo, Egypt, in 1964. He received his B.Sc. and M.Sc. degrees in electrical engineering from Ain Shams University, Cairo, Egypt, in 1986 and 1990, respectively, and his Ph.D. degree in electrical engineering from the University of Waterloo, Waterloo, ON, Canada, in 1998, where he was a professor with the ECE Department till 2019, where he was the director of the Power MEng program between 2010 and 2015. Currently, he is a professor of the Department of Electrical Engineering and the dean of the college of engineering and physical sciences at Khalifa University, UAE. Dr. El-Saadany is an internationally recognized expert in the area of sustainable energy integration and smart distribution systems. His research interests include smart grid operation and control, microgrids, transportation electrification, self-healing, cyber-physical security of smart grids, protection, power quality, and embedded generation. He is registered professional engineer in the province of Ontario.

REFERENCES

[1] Natural Resources Canada (NRCan), "The atlas of Canada—remote communities energy database," [Online]. Available: https://atlas.gc.ca/rced-bdece/en/index.html

[2] N. Pogaku, M. Prodanovic, and T. C. Green, "Modeling, analysis and testing of autonomous operation of an inverter-based microgrid," *IEEE Transactions on Power Electronics*, vol. 22, no. 2, pp. 613-625, Mar. 2007.

[3] A. Cagnano, E. De Tuglie, and P. Mancarella, "Microgrids: overview and guidelines for practical implementations and operation," *Applied Energy*, vol. 258, Jan. 2020.

[4] M. Farrokhabadi, C. A. Cañizares, and K. Bhattacharya, "Frequency control in isolated/islanded microgrids through voltage regulation," *IEEE Transactions on Smart Grid*, vol. 8, no. 3, pp. 1185-1194, May 2017.

[5] T. Alharbi and K. Bhattacharya, "Optimal scheduling of energy resources and management of loads in isolated/islanded microgrids," *Canadian Journal of Electrical and Computer Engineering*, vol. 40, no. 4, pp. 284-294, Dec. 2017.

[6] X. Ge, Q. Han, and L. Ding *et al.*, "Dynamic event-triggered distributed coordination control and its applications: a survey of trends and techniques," *IEEE Transactions on Systems*, *Man*, *and Cybernetics*: *Systems*, vol. 50, no. 9, pp. 3112-3125, Sep. 2020.

[7] T. E. Sati, M. A. Azzouz, and M. F. Shaaban, "Adaptive harmonic-based protection coordination for inverter-dominated isolated microgrids considering N-1 contingency," *International Journal of Electrical Power & Energy Systems*, vol. 156, Feb. 2024.

[8] W. T. El-Sayed, H. E. Z. Farag, and H. H. Zeineldin *et al*., "Formation of islanded droop-based microgrids with optimum loadability," *IEEE Transactions on Power Systems*, vol. 37, no. 2, pp. 1564-1576, Mar. 2022.

[9] A. A. Eajal, A. H. Yazdavar, and E. F. El-Saadany *et al*., "On the loadability and voltage stability of islanded AC-DC hybrid microgrids during contingencies," *IEEE Systems Journal*, vol. 13, no. 4, pp. 4248-4259, Dec. 2019.

[10] Y. Weng, R. Rajagopal, and B. Zhang, "A geometric analysis of power system loadability regions," *IEEE Transactions on Smart Grid*, vol. 11, no. 4, pp. 3580-3592, Jul. 2020.

[11] M. M. A. Abdelaziz and E. F. El-Saadany, "Maximum loadability consideration in droop-controlled islanded microgrids optimal power flow," *Electric Power Systems Research*, vol. 106, pp. 168-179, Jan. 2014.

[12] M. M. A. Abdelaziz, H. E. Farag, and E. F. El-Saadany, "Optimum droop parameter settings of islanded microgrids with renewable energy resources," *IEEE Transactions on Sustainable Energy*, vol. 5, no. 2, pp. 434-445, Apr. 2014.

[13] M. A. Allam, A. A. Hamad, and M. Kazerani *et al*., "A novel dynamic power routing scheme to maximize loadability of islanded hybrid AC/DC microgrids under unbalanced AC loading," *IEEE Transactions on Smart Grid*, vol. 9, no. 6, pp. 5798-5809, Nov. 2018.

[14] A. M. Tahboub, V. R. Pandi, and H. H. Zeineldin, "Distribution system reconfiguration for annual energy loss reduction considering variable distributed generation profiles," *IEEE Transactions on Power Delivery*, vol. 30, no. 4, pp. 1677-1685, Aug. 2015.

[15] Y. Fu and H. Chiang, "Toward optimal multiperiod network reconfiguration for increasing the hosting capacity of distribution networks," *IEEE Transactions on Power Delivery*, vol. 33, no. 5, pp. 2294-2304, Oct. 2018.

[16] S. M. Razavi, H. R. Momeni, and M. R. Haghifam *et al*., "Multi-objective optimization of distribution networks via daily reconfiguration," *IEEE Transactions on Power Delivery*, vol. 37, no. 2, pp. 775-785, Apr. 2022.

[17] B. Venkatesh, R. Ranjan, and H. B. Gooi, "Optimal reconfiguration of radial distribution systems to maximize loadability," *IEEE Transactions on Power Systems*, vol. 19, no. 1, pp. 260-266, Feb. 2004.

[18] M. M. A. Abdelaziz, H. E. Farag, and E. F. El-Saadany, "Optimum reconfiguration of droop-controlled islanded microgrids," *IEEE Transactions on Power Systems*, vol. 31, no. 3, pp. 2144-2153, May 2016.

[19] J. Kim and Y. Dvorkin, "Enhancing distribution system resilience with mobile energy storage and microgrids," *IEEE Transactions on Smart Grid*, vol. 10, no. 5, pp. 4996-5006, Sep. 2019.

[20] W. Wang, X. Xiong, and Y. He *et al*., "Scheduling of separable mobile energy storage systems with mobile generators and fuel tankers to boost distribution system resilience," *IEEE Transactions on Smart Grid*, vol. 13, no. 1, pp. 443-457, Jan. 2022.

[21] M. Nazemi, P. Dehghanian, and X. Lu *et al*., "Uncertainty-aware deployment of mobile energy storage systems for distribution grid resilience," *IEEE Transactions on Smart Grid*, vol. 12, no. 4, pp. 3200-3214, Jul. 2021.

[22] S. Yao, P. Wang, and X. Liu *et al*., "Rolling optimization of mobile energy storage fleets for resilient service restoration," *IEEE Transactions on Smart Grid*, vol. 11, no. 2, pp. 1030-1043, Mar. 2020.

[23] W. T. Elsayed, H. Farag, and H. H. Zeineldin *et al*., "Dynamic transitional droops for seamless line-switching in islanded microgrids," *IEEE Transactions on Power Systems*, vol. 36, no. 6, pp. 5590-5601, Nov. 2021.

[24] E. E. Pompodakis, G. C. Kryonidis, and M. C. Alexiadis *et al*., "A Three-phase sensitivity-based approach for smooth line-switching in islanded networks," *International Journal of Electrical Power & Energy Systems*, vol. 144, Jan. 2023.

[25] A. Zhou, H. Zhai, and M. Yang *et al*., "Three-phase unbalanced distribution network dynamic reconfiguration: a distributionally robust approach," *IEEE Transactions on Smart Grid*, vol. 13, no. 3, pp. 2063-2074, May 2022.

[26] Z. N. Popovic and S. D. Knezevic, "Dynamic reconfiguration of distribution networks considering hosting capacity: a risk-based approach," *IEEE Transactions on Power Systems*, Vol. 8, no. 4, pp. 3440-3450, Jul. 2023.

[27] M. R. Dorostkar-Ghamsari, M. Fotuhi-Firuzabad, and M. Lehtonen *et al*., "Value of distribution network reconfiguration in presence of renewable energy resources," *IEEE Transactions on Power Systems*, vol. 31, no. 3, pp. 1879-1888, May 2016.

[28] S. Golshannavaz, S. Afsharnia, and F. Aminifar, "Smart distribution grid: optimal day-ahead scheduling with reconfigurable topology," *IEEE Transactions on Smart Grid*, vol. 5, no. 5, pp. 2402-2411, Sep. 2014.

[29] S. Talukder, M. Ibrahim, and R. Kumar, "Resilience indices for power/cyberphysical systems," *IEEE Transactions on Systems*, *Man*, *and Cybernetics*: *Systems*, vol. 51, no. 4, pp. 2159-2172, Apr. 2021.

[30] M. Panteli, P. Mancarella, and D. N. Trakas *et al*., "Metrics and quantification of operational and infrastructure resilience in power systems," *IEEE Transactions on Power Systems*, vol. 32, no. 6, pp. 4732-4742, Nov. 2017.

[31] M. E. Baran and F. Wu, "Network reconfiguration in distribution systems for loss reduction and load balancing," *IEEE Transactions on Power Delivery*, vol. 4, no. 2, pp. 1401-1407, Apr. 1989.

[32] H. M. A. Ahmed, H. F. Sindi, and M. A. Azzouz *et al.*, "Optimal sizing and scheduling of mobile energy storage toward high penetration levels of renewable energy and fast charging stations," *IEEE Transactions on Energy Conversion*, vol. 37, no. 2, pp. 1075-1086, Jun. 2022.

[33] S. Lei, C. Chen, and H. Zhou *et al*., "Routing and scheduling of mobile power sources for distribution system resilience enhancement," *IEEE Transactions on Smart Grid*, vol. 10, no. 5, pp. 5650-5662, Sep. 2019.

[34] H. H. Abdeltawab and Y. A.-R. I. Mohamed, "Mobile energy storage scheduling and operation in active distribution systems," *IEEE Transactions on Industrial Electronics*, vol. 64, no. 9, pp. 6828-6840, Sep. 2017.